




Article

Production of Biofuel Additives Using Catalytic Bioglycerol Etherification: Kinetic Modelling and Reactive Distillation Design

Abdulrahman A. Al-Rabiah ^{1,*} , Rayan K. Al Darwish ¹ , Abdullah E. Alqahtani ¹, Diego Morais Chaves ² and Márcio J. da Silva ² 

¹ Chemical Engineering Department, College of Engineering, King Saud University, Riyadh 11421, Saudi Arabia

² Chemistry Department, Federal University of Viçosa, Viçosa 36570-900, Brazil

* Correspondence: arabiah@ksu.edu.sa

Abstract: Glycerol is an unavoidable by-product of the biodiesel production process. The conversion of glycerol into valuable biofuel additives is essential in the fuel industry. The goal of this work is to develop a reactive distillation-based process for the production of biofuel additives by bio-glycerol etherification. In this study, a kinetic model using a lumping approach for glycerol etherification with *tert*-butyl alcohol (TBA) over Sn (II) phosphomolybdate (Sn_{1.5}PMo₁₂O₄₀) catalyst was developed. Aspen Plus was used to validate the kinetic model by simulating the glycerol etherification with TBA in a batch reactor. The model predictions were in good agreement with the experimental data. A reactive distillation-based process to produce glycerol ethers was developed, and heat integration was conducted to reduce energy consumption. The energy requirements of the integrated process and the CO₂ emissions were decreased by 17% and 14%, respectively. An economic evaluation was performed to study the profitability of the process for an annual capacity of 33,000 metric tons of glycerol ethers. It was found that the process is economically attractive, with a return on investment of 29.40% and a payback period of 2.2 years. The reactive distillation-based process is green and promising for producing biofuel additives that are sustainable and environmentally friendly.

Keywords: glycerol; etherification; *tert*-butyl alcohol; kinetic modeling; reactive distillation; process integration; catalytic reaction



Citation: Al-Rabiah, A.A.; Al Darwish, R.K.; Alqahtani, A.E.; Chaves, D.M.; da Silva, M.J. Production of Biofuel Additives Using Catalytic Bioglycerol Etherification: Kinetic Modelling and Reactive Distillation Design. *Catalysts* **2022**, *12*, 1332. <https://doi.org/10.3390/catal12111332>

Academic Editors: Mohamed Mokhtar M. Mostafa, Tamer S. Saleh and Nesreen S. Ahmed

Received: 24 September 2022

Accepted: 24 October 2022

Published: 1 November 2022

Publisher's Note: MDPI stays neutral with regard to jurisdictional claims in published maps and institutional affiliations.



Copyright: © 2022 by the authors. Licensee MDPI, Basel, Switzerland. This article is an open access article distributed under the terms and conditions of the Creative Commons Attribution (CC BY) license (<https://creativecommons.org/licenses/by/4.0/>).

1. Introduction

Oxygenated additives are well known for producing cleaner-burning diesel fuels by increasing oxygen levels and the octane rating number of the fuel. In addition, additives decrease the fuel vapor pressure, which in turn limits carbon emissions [1–3]. In recent years, glycerol ethers have been considered promising oxygenated additives for diesel fuels [4]. The blending of glycerol ethers with diesel enhances internal combustion efficiency, decreases pollutant emissions, and improves fuel properties such as pour and cloud points [5].

Biodiesel is produced by the transesterification process in which vegetal oils react with alcohol in the presence of alkaline-based catalysts [6–8]. The biodiesel process produces glycerol as a by-product, consisting of ~10 wt.% of the total fuel [9–11]. The high demand for biodiesel has created an abundant supply of glycerol, which has caused the prices of glycerol to decline [12]. Accordingly, research efforts have been developed to make a more sustainable and economically viable biodiesel production process using different routes for converting glycerol into value-added chemicals [13].

One promising process is the conversion of glycol to ethers. The glycerol ethers are oxygenated additives with attractive properties. Mono-*tert*-butyl glycerol ether (MTBG) is typically used as an efficient surfactant, while di-*tert*-butyl glycerol ether (DTBG) and

tri-*tert*-butyl glycerol ether (TTBG) are used as alternatives to replace conventional fuel additives such as methyl *tert*-butyl ether (MTBE), which has a fossil origin [14,15].

Glycerol etherification can be carried out using isobutylene or *tert*-butyl alcohol (TBA), and it was concluded that TBA is preferable compared to isobutylene [16]. In addition, isobutylene is in the gas phase during the reaction with glycerol, while TBA and glycerol are both in the liquid phase. Therefore, the use of TBA prevents oligomerization and overcomes the need for an additional solvent during the etherification reaction [8,10,16,17]. In most cases, heterogeneous solid catalysts are preferable for glycerol etherification over homogenous catalysts, and this is because homogeneous catalysts are known for their high operational costs and environmental drawbacks [18,19]. Many studies were carried out with solid catalysts for glycerol etherification using TBA to maximize conversion and selectivity. The heterogeneous catalysts include ion exchange resins, zeolites, sulfonated niobium oxides, a pillared clay, sulfonic acid-functionalized mesoporous polymers, sulfonated hybrid silicas, and amorphous organosilica-aluminium phosphates [16,20–23]. Da Silva et al. studied the synthesis of three Keggin heteropolyacid salts doped with different Sn (II) amounts to evaluate their performance as catalysts for glycerol etherification with TBA [24]. It was found that $\text{Sn}_{1.5}\text{PMo}_{12}\text{O}_{40}$ provided the maximum selectivity toward DTBG and greater conversion among the three Keggin heteropolyacid salts.

Several studies have attempted to develop kinetic models that accurately describe the etherification of glycerol using TBA over different catalysts, but none was done for the $\text{Sn}_{1.5}\text{PMo}_{12}\text{O}_{40}$. Frusteri et al. developed a simple kinetic model that represents the reaction of glycerol with TBA catalyzed by Amberlyst 15 [8]. The reaction order was determined using the excess method conditions. Pico et al. developed both lumped and extended kinetic models for glycerol etherification with TBA catalyzed by Amberlyst 15 [10]. The lumped model contains three stoichiometric reaction equations, while the extended model has six stoichiometric reaction equations. It was reported that the two kinetic models provided a good representation of the experimental reactions.

Reactive distillation (RD) is considered a well-researched multi-functional technique for industrial applications due to its advantages which include reduced cost, improved separation process, improved selectivity, less energy consumption, and less complicated processes [25]. In addition, RD allows that chemical reaction and separation to occur at the same time inside the column, avoiding problems of equilibrium limitations that are common in a plethora of reversible reactions [26]. Even though other studies in the literature investigated etherification reactions, none of them developed a complete industrial-scale process for producing glycerol ethers using a reactive distillation-based process [15–17,27].

In this work, a kinetic model of glycerol etherification with TBA using the $\text{Sn}_{1.5}\text{PMo}_{12}\text{O}_{40}$ catalyst will be derived. A reactive distillation-based process will be developed to produce glycerol ethers from a catalytic etherification reaction with TBA. A heat integration will be carried out to reduce the energy consumption and CO_2 emissions of the reactive distillation-based process. The feasibility of the process will be verified through an economic analysis.

2. Results and Discussion

The diffractograms of phosphomolybdic acid and its tin salt are shown in Figure 1. It can be noticed that acid has greater crystallinity than Sn salt. However, the diffraction peaks were seen at the same 2θ angle. It is suggestive that the secondary structure of the Keggin anion was maintained even after the replacement of protons by Sn^{2+} cations.

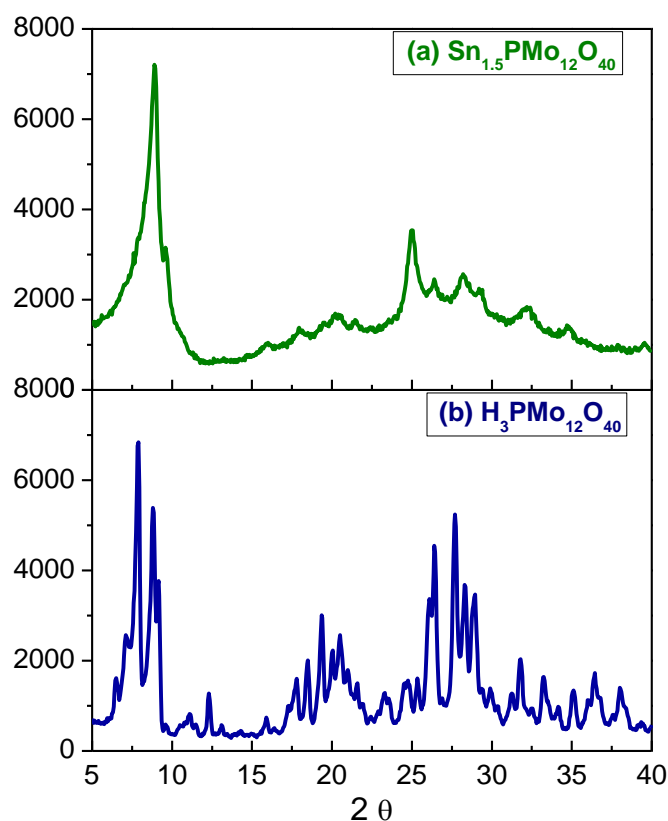


Figure 1. Diffractograms of (a) $\text{Sn}_{1.5}\text{PMo}_{12}\text{O}_{40}$ catalyst and (b) its precursor $\text{H}_3\text{PMo}_{12}\text{O}_{40}$.

The diffraction peaks noticed in the diffractogram of tin phosphomolybdate salt underwent enlargement and loss of intensity triggered by the presence of Sn (II) cation. The crystallite size was calculated by Scherrer Equation (Equation (1)), where λ corresponds to the Cu $\text{K}\alpha$ radiation, and β is the full width at half-maximum for a reflection maximum located at 2θ .

$$L = \frac{0.9 \lambda}{\beta \cos \theta} \quad (1)$$

The protons exchange by Sn^{2+} led to a lower crystallite size (25.5 to 9.9 nm; phosphomolybdic acid and its tin salt, respectively). These measurements were performed in duplicate.

The elemental composition of tin phosphomolybdate was confirmed through energy dispersive spectroscopy. It was compared to the pristine heteropolyacid in Table 1.

Table 1. Energy dispersive spectroscopy analysis of $\text{Sn}_{1.5}\text{PMo}_{12}\text{O}_{40}$ catalyst and its precursor $\text{H}_3\text{PMo}_{12}\text{O}_{40}$ *.

| Mass (%) | $\text{H}_3\text{PMo}_{12}\text{O}_{40}$ | | $\text{Sn}_{1.5}\text{PMo}_{12}\text{O}_{40}$ | |
|----------|--|------|---|------|
| | Theoretical | EDS | Theoretical | EDS |
| H | 0.2 | - | 0 | - |
| Sn | 0 | 0 | 8.5 | 9.5 |
| P | 1.7 | 2.3 | 1.5 | 2.4 |
| Mo | 63.1 | 62.1 | 58.0 | 57.7 |
| O | 35.0 | 35.6 | 32.0 | 30.4 |

* the values presented are the average of three different regions of the catalyst surface.

There was a satisfactory agreement between theoretical and experimental values for both compounds, assuring the synthesis was carried out with success. Since EDS was

coupled to an electronic scan microscope, the images of the catalyst surface were obtained and shown in Figure 2.

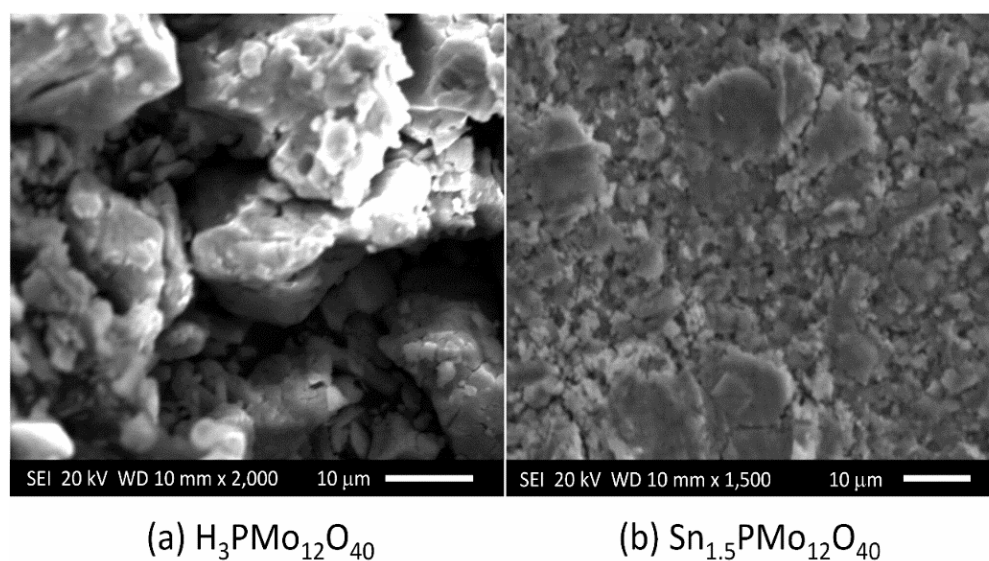


Figure 2. SEM images of (a) Precursor $\text{H}_3\text{PMo}_{12}\text{O}_{40}$ and (b) $\text{Sn}_{1.5}\text{PMo}_{12}\text{O}_{40}$ catalyst.

As verified by the Sherrer equation, the particle size of $\text{Sn}_{1.5}\text{PMo}_{12}\text{O}_{40}$ was smaller than pristine acid. From the N_2 adsorption/desorption isotherms (Figure 3), the surface properties of tin phosphomolybdate were obtained. Table 2 shows that they were very close to those obtained from phosphomolybdic acid.

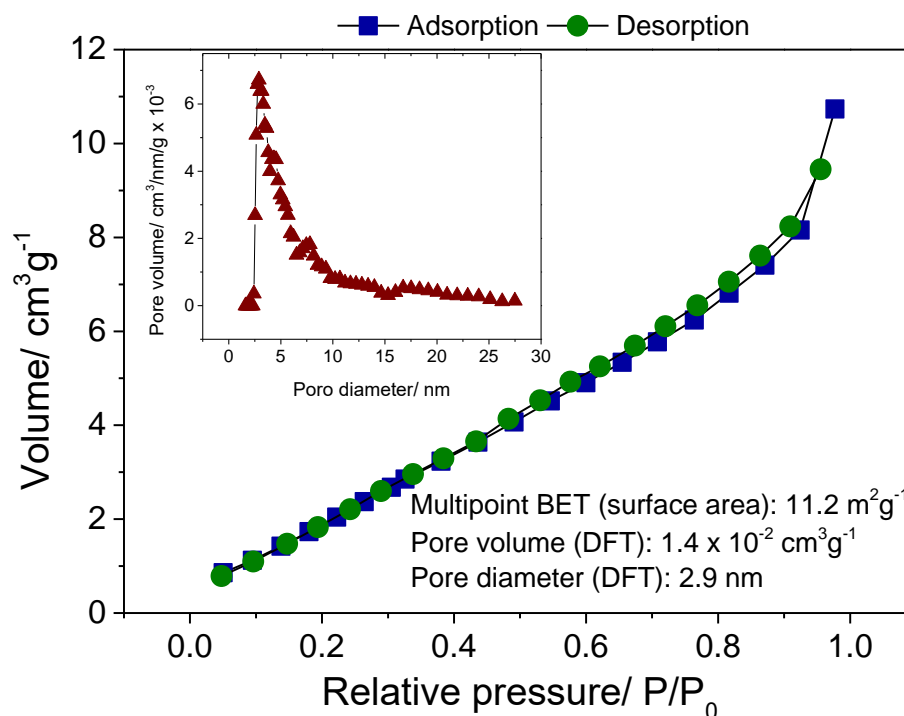
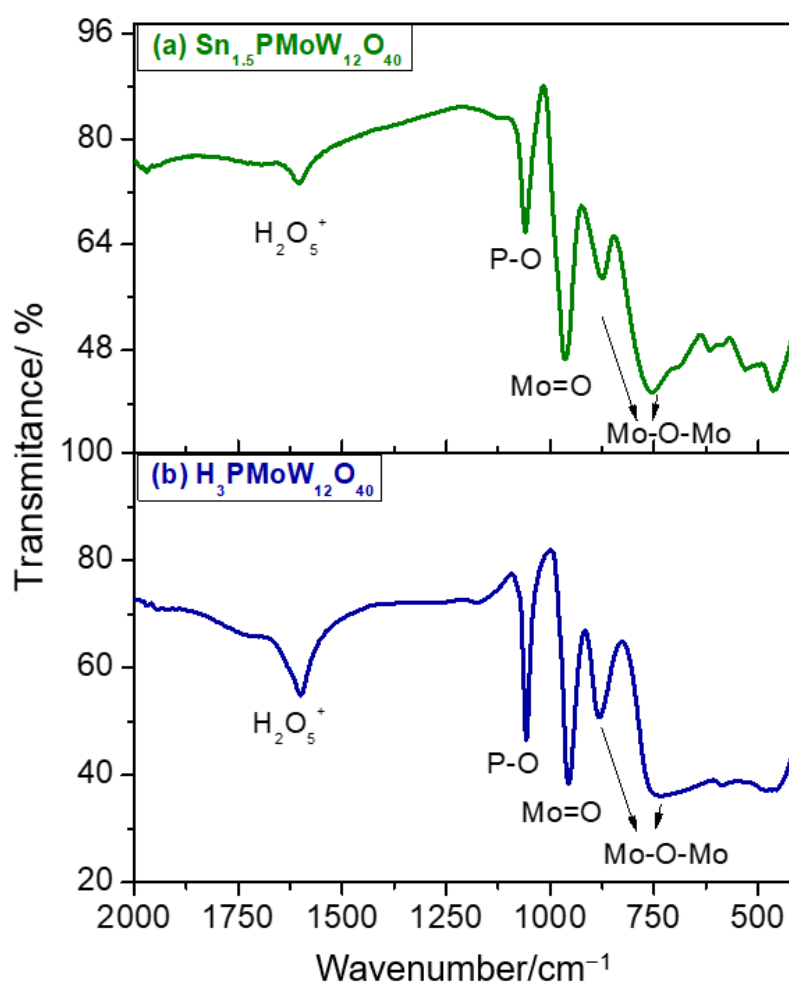


Figure 3. Texture properties of $\text{Sn}_{1.5}\text{PMo}_{12}\text{O}_{40}$ catalyst: N_2 adsorption and desorption curves and pores diameter distribution curve.

Table 2. Texture properties of $\text{H}_3\text{PMo}_{12}\text{O}_{40}$ and $\text{Sn}_{1.5}\text{PMo}_{12}\text{O}_{40}$ salt.

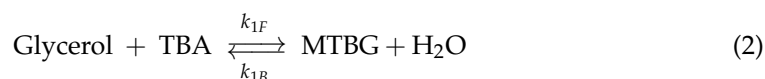
| Catalyst | Surface Area $\text{m}^2 \text{g}^{-1}$ | Pore Volume ($\times 10^{-2} \text{cm}^3/\text{g}$) | Pore Diameter (nm) |
|---|--|--|-----------------------|
| $\text{H}_3\text{PMo}_{12}\text{O}_{40}$ | 11.8 | 1.7 | 3.8 |
| $\text{Sn}_{1.5}\text{PMo}_{12}\text{O}_{40}$ | 11.2 | 1.4 | 2.9 |

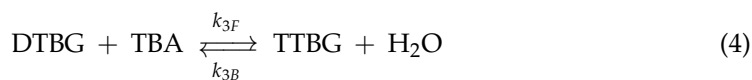
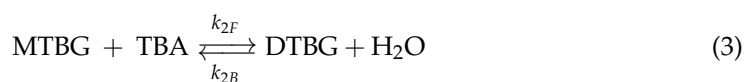
The infrared spectra of phosphomolybdic acid and its tin salt are shown in Figure 4. The main absorption bands noticed in the spectrum of $\text{H}_3\text{PMo}_{12}\text{O}_{40}$ acid were placed at 1015, 977, 910, and 760 cm^{-1} wavenumbers, which were attributed to the vibrations of ν_{as} P-O, ν_{as} Mo=O, ν_{as} Mo-O_v-Mo, and ν_{as} Mo-O_a-Mo, respectively. These same absorption bands were also observed in the spectrum of tin phosphomolybdate. This observation suggests that after the protons exchange of pristine heteropolyacid, its Keggin structure was preserved.

**Figure 4.** FTIR spectra of (a) $\text{Sn}_{1.5}\text{PMo}_{12}\text{O}_{40}$ and (b) its precursor $\text{H}_3\text{PMo}_{12}\text{O}_{40}$.

2.1. Kinetic Modelling

A kinetic model of the glycerol etherification with TBA over the $\text{Sn}_{1.5}\text{PMo}_{12}\text{O}_{40}$ catalyst was derived by the lumping approach [7,8]. The forward (k_{1F}) and backward (k_{1B}) reaction rate constants where $n = 1, 2$, or 3 are shown in Equations (2)–(4):





A power law approach was used to model the reaction kinetics, and the rate equations are second-order, as shown in Equations (5)–(7), where “C” refers to the concentration of a specific reactant:

$$r_1 = k_{1F}C_G C_{TBA} - k_{1B}C_{MTBG}C_{H_2O} \quad (5)$$

$$r_2 = k_{2F}C_{MTBG}C_{TBA} - k_{2B}C_{DTBG}C_{H_2O} \quad (6)$$

$$r_3 = k_{3F}C_{DTBG}C_{TBA} - k_{3B}C_{TTBG}C_{H_2O} \quad (7)$$

The Arrhenius equation that describes the temperature dependence of the reaction rates is shown in Equation (8), where “ k_{0i} ” is the pre-exponential factor:

$$k_i = k_{0i} e^{-\frac{E_i}{RT}} \quad (8)$$

The reaction rate constants have been determined by plotting the inverse of concentration versus time. The mass balance equations of the reactants and products are shown in Table 3. The kinetic model is based on reaction stoichiometry. When one mol of glycerol is consumed, one mol of MTBG and one mol of water are formed. Consequently, when this is converted to DTBG, one mol of water is formed. The same occurs when DTBG is converted to TTBG (see Equations (1)–(3)). Glycerol is only consumed by r_1 , and TBA is consumed by r_1 , r_2 , and r_3 . MTBG, on the other hand, is generated by r_1 and consumed by r_2 , DTBG is generated by r_2 and consumed by r_3 , and TTBG is generated by r_3 .

Table 3. Mass balances of the reactants and products.

| Component | Mass Balance Equation | Component | Mass Balance Equation |
|-----------|--|-----------|------------------------------------|
| Glycerol | $\frac{dC_G}{dt} = -r_1$ | DTBG | $\frac{dC_{DTBG}}{dt} = r_2 - r_3$ |
| TBA | $\frac{dC_{TBA}}{dt} = -r_1 - r_2 - r_3$ | TTBG | $\frac{dC_{TTBG}}{dt} = r_3$ |
| MTBG | $\frac{dC_{MTBG}}{dt} = r_1 - r_2$ | | |

The Arrhenius equation was used to find the pre-exponential (frequency) factors (k_{0i}) and the activation energies (E_i), as listed in Table 4. The concentrations of glycerol and products obtained experimentally at different temperatures were used to find (k_{0i}) and (E_i).

Table 4. Frequency factors (k_0) and activation energies (E_a) of the kinetic model.

| Pre-Exponential Factor (m ³ /mol·s) | | Activation Energy (kJ/mol) | |
|--|-------------------|----------------------------|------|
| k_{0_1F} | 6.8×10^8 | E_{1F} | 91 |
| k_{0_1B} | 7×10^3 | E_{1B} | 52.5 |
| k_{0_2F} | 2×10^6 | E_{2F} | 61 |
| k_{0_2B} | 3×10^3 | E_{2B} | 30 |
| k_{0_3F} | 0.7×10^3 | E_{3F} | 66 |
| k_{0_3B} | 0.1×10^3 | E_{3B} | 80 |

A batch reactor (RBatch) model of Aspen Plus was used to simulate the three reactions. The simulation results were validated and compared with the experimental data obtained from the work of Da Silva et al. [24]. The batch reactor has an initial amount of glycerol and TBA of 0.0046 mol and 0.0368 mol, respectively. The reactor was simulated at an isothermal

temperature of 363 K, and the pressure was gradually increased from 1.0 bar to 3.8 bar for a 4-h duration.

Figure 5 shows the molar compositions of the experimental data and the simulation results plotted versus time for glycerol, MTBG, DTBG, and TTBG. Results in Figure 5 show that only 67% of conversion was achieved under these reaction conditions. Moreover, almost no TTBG was formed. It suggests that the performance of this catalyst using these conditions was not satisfactory when using the conventional reactor.

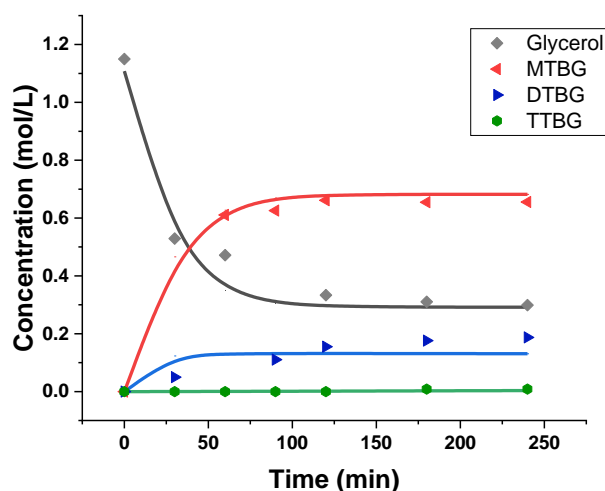


Figure 5. Experimental molar concentrations (symbols) and kinetic simulations (lines) as a function of time at 363 K and a reaction time of 8 h.

Figure 6 shows a parity diagram of glycerol conversions and product selectivities. In the parity diagram, the data obtained using the developed model has been plotted as a function of the experimental data. It was found that the kinetic model provided a good agreement with the experimental data in the range of $\pm 10\%$. The straight-line correlation coefficient, R^2 , equals 0.9739.

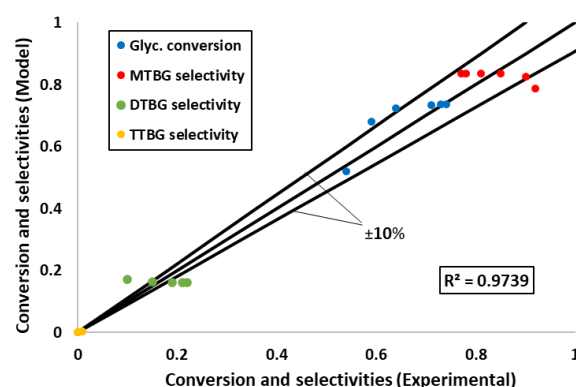


Figure 6. Parity graph of the experimental data and theoretical data (model) of glycerol conversion and product selectivities.

2.2. Reactive Distillation Design

A reactive distillation (RD) column has been designed and simulated using RadFrac of Aspen Plus (version 11, AspenTech, Bedford, MA, USA) software for glycerol etherification with TBA using $\text{Sn}_{1.5}\text{PMo}_{12}\text{O}_{40}$ as a catalyst to produce glycerol ethers. The reactive distillation column is used to shift the equilibrium of the etherification reactions toward the more desirable products (i.e., DTBG and TTBG). When using a conventional reactor, the reaction route favors the MTBG, which is less valuable.

The NRTL model was used for activity coefficients due to the nonideal vapor-liquid equilibrium and the presence of an azeotropic mixture in the process (TBA/water). As illustrated in Figure 7, the RD column consists of 20 sieve stages and six reactive stages, which start from stage 5 to stage 10. The RD column has a total condenser and a kettle reboiler. The glycerol is fed at the 5th stage of the RD column with a flow rate of 20 kmol/h at 363 K and 3.8 bar, while the TBA is fed at the bottom of the RD column with a flow rate of 100 kmol/h at 363 K and 4.1 bar. The ratio of glycerol to TBA was set to 5. Water and TBA are separated at the RD column's overhead, while glycerol ethers are separated in the bottom stream. The unreacted glycerol is about 0.6 mol%. It was found that the MTBG was entirely converted to DTBG.

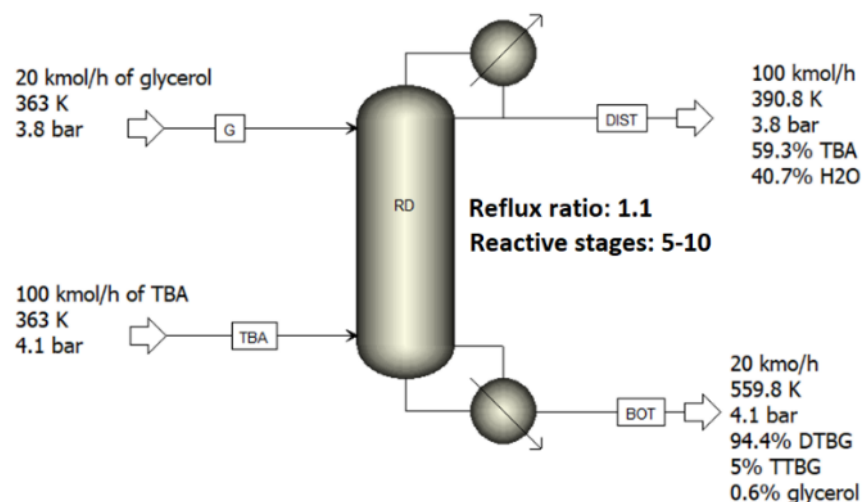


Figure 7. Reactive distillation column for glycerol etherification with TBA (reflux ratio = 1.1, Reactive stages = 6, TBA:Gly = 5).

A parametric study was performed to evaluate the effect of the reflux ratio on the conversion of glycerol. The flow rate of the unreacted glycerol is plotted at different reflux ratios, as shown in Figure 8a. The unreacted glycerol varies from 0.13 to 0.63 kmol/h. The maximum glycerol conversion (~99%) occurred when the reflux ratio was in the range of 0.9–1.3. Figure 8b shows the molar fractions of the glycerol ethers (i.e., MTBG, DTBG, TTBG) as a function of the reflux ratio. It was found that for the reflux ratio above 0.4, the desired products are only DTBG and TTBG that are present in the bottom stream, while the undesired product (MTBG) is completely consumed.

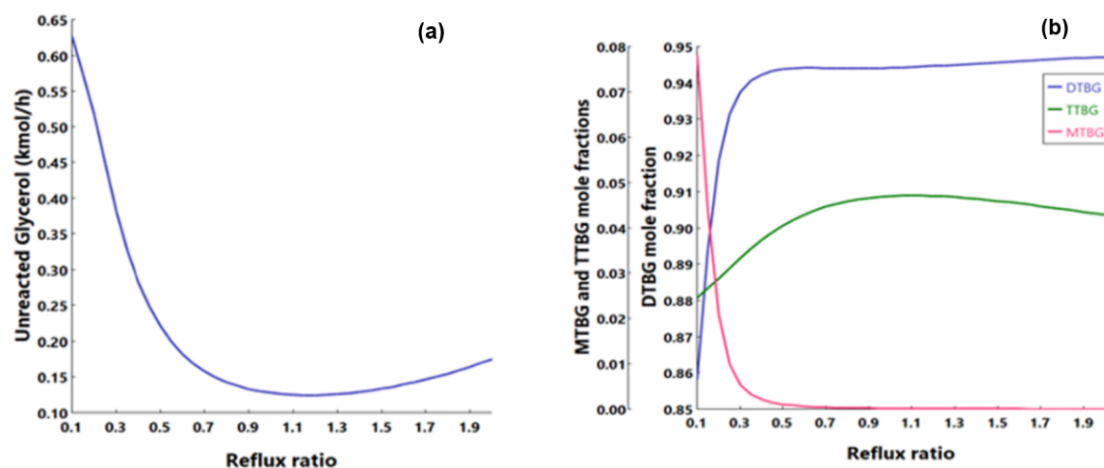


Figure 8. For reactive stages = 6, TBA: Gly = 5, (a) unreacted glycerol flow rate as a function of the reflux ratio, and (b) glycerol ether compositions in the bottom stream as a function of the reflux ratio.

The rectifying section is necessary to achieve higher conversion by removing water from the column [28]. The reactive zone starts after the rectifying section at the 5th stage, and a parametric study was done to identify the optimum number of stages in the reactive zone. The effect of the number of reactive stages on glycerol conversion and product purity is shown in Figure 9a,b, respectively. The increase in the number of reactive stages increases the glycerol conversion and consequently reduces the unreacted glycerol at the bottom. The maximum conversion is attained using six reactive stages, starting at the 5th stage and ending at the 10th stage.

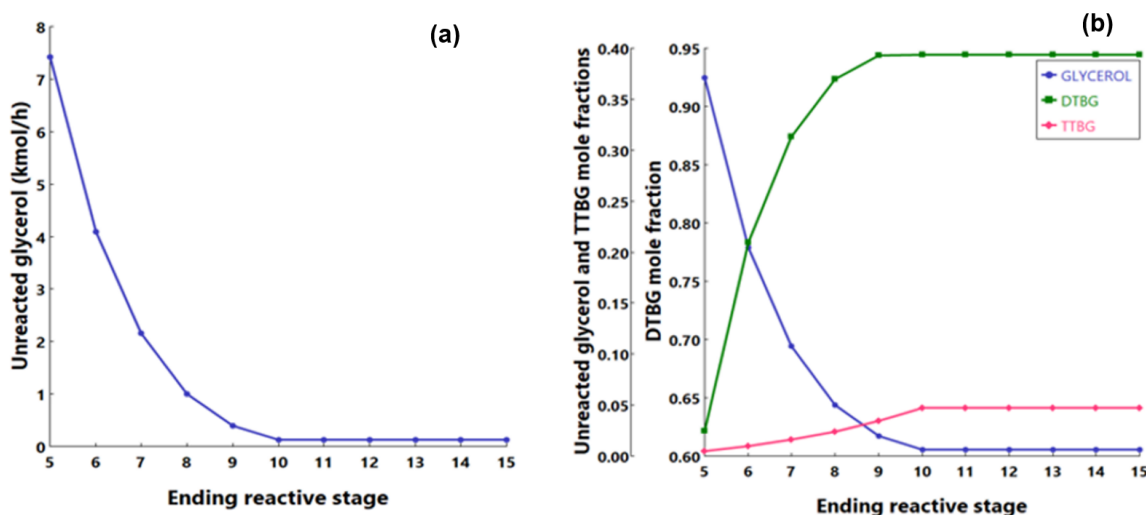


Figure 9. For Reflux ratio = 1.1, TBA:Gly = 5, (a) Unreacted glycerol flow rate at the bottom stream as a function of reactive stages. (b) Glycerol, DTBG, and TTBG mole fractions in the bottom stream as a function of reactive stages.

The effects of feed ratio (TBA: Glycerol) on glycerol conversion and product mole fractions are shown in Figure 10a,b, respectively. The TBA flow rate varied from 20–150 kmol/h for a feed ratio (TBA: Glycerol) of 1 to 7.5. When the TBA flow rate is increased, the conversion of glycerol increases until the TBA feed flow rate is 100 kmol/h (TBA: Glycerol ratio = 5), when glycerol is completely consumed.

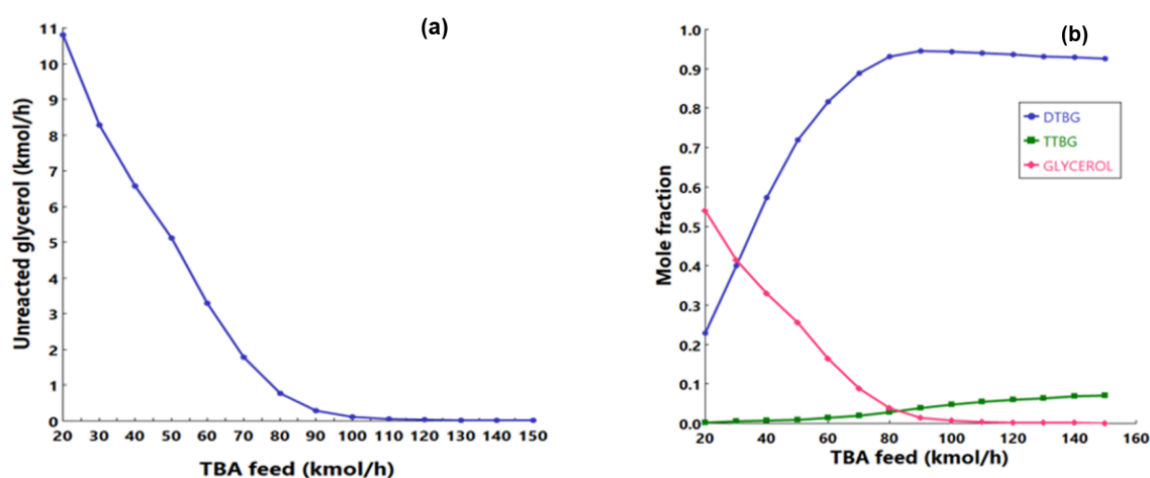


Figure 10. For Reflux ratio = 1.1, reactive stages = 6, (a) Unreacted glycerol in the bottom stream as a function of TBA feed flow rate, (b) Unreacted glycerol, DTBG, and TTBG mole fractions in the bottom stream as a function of TBA feed flow rate.

2.3. Process Development

The reactive distillation-based process for the production of glycerol ethers is shown in Figure 11. The process was developed and simulated using Aspen Plus® for a typical plant capacity of 33,000 metric tons per year. Glycerol feed (stream 1) of 20 kmol/h is pumped using P-101 at 3.8 bar and heated in heat exchanger E-101 at 363 K. The glycerol enters the reactive distillation column at the top stage. TBA fresh feed (stream 3) is mixed with the recycled TBA (stream 10) and pumped using P-102 at 4.1 bar. The TBA is heated using E-101 at 363 K and fed to the RD column at the bottom stage with a flow rate of 100 kmol/h.

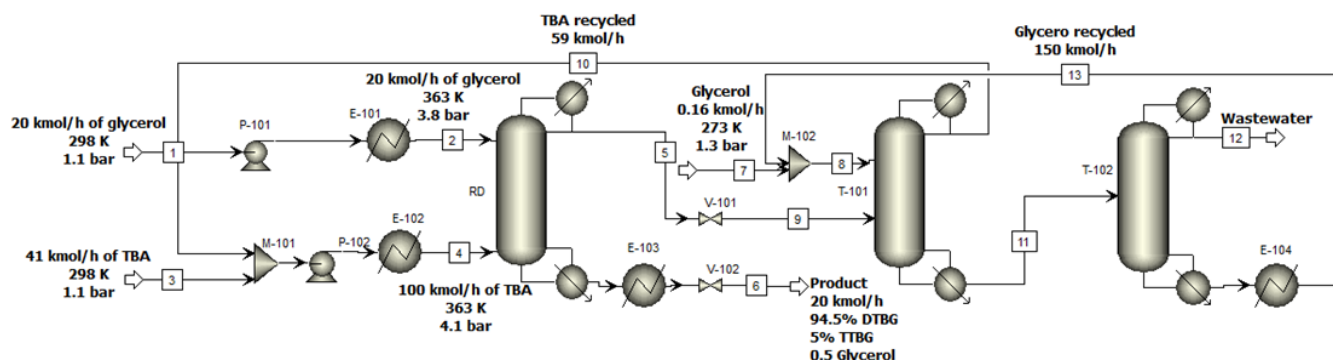


Figure 11. Process flow diagram (PFD) of the glycerol etherification with TBA using reactive distillation.

The conversion of glycerol in the RD column is ~99%. The glycerol ethers (DTBG and TTBG) are separated at the bottom of the column. The product is cooled in E-103 at 298 K (stream 6) and sent to the storage tank. The glycerol ethers consist of DTBG (94.5 mol%) and TTBG (5 mol%). The overall purity of the glycerol ethers is 99.5 mol%. °C

Water and unreacted TBA are separated at the top of the RD column (stream 5). The residue curve map of the TBA-water-glycerol mixture is shown in Figure 12. Water and TBA are saddles, and glycerol is the stable node. The azeotrope, the unstable node, happens when the mixture has 62.1% TBA and 37.9% water.

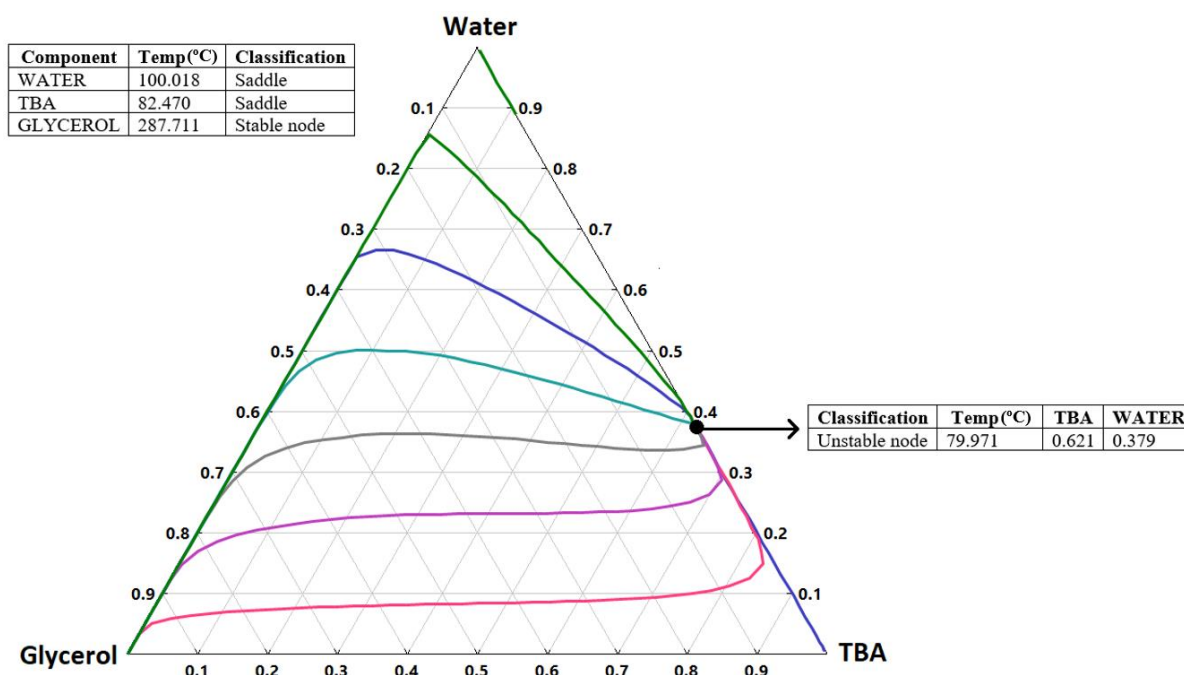


Figure 12. Residue curves map of the TBA-water-glycerol mixture at a pressure of 1 bar.

The azeotropic mixture of the TBA and water is sent to an extractive distillation unit (T-101) for purification. Glycerol is used as a solvent and fed at the top of the extractive distillation column with a flow rate of 150 kmol/h. A water-TBA mixture is fed at the 15th stage of the extractive distillation column with a flow rate of 100 kmol/h (stream 9). TBA exits the extractive distillation column as the distillate with a flow rate of 59 kmol/h (stream 10), which is recycled back and mixed with the fresh feed of TBA. The glycerol-water mixture leaves the extractive distillation in the bottom stream and is sent to the solvent recovery column (T-102). Glycerol solvent is recovered in the bottom stream and sent back to the extractive distillation column (T-101). Table 5 shows the stream information of the process.

Table 5. Streams information of glycerol with TBA etherification process.

| Stream | 1 | 2 | 3 | 4 | 5 | 6 | 7 |
|--|---------|-------|-------|---------|-------|---------|-----|
| Temperature (K) | 298 | 363 | 298 | 363 | 391 | 308 | 298 |
| Pressure (bar) | 1 | 4 | 1 | 4 | 4 | 2 | 1 |
| Enthalpy flow (kW) | −3708 | −3635 | −4119 | −9530 | −8670 | −4201 | −30 |
| Vapor mole fraction | 0 | 0 | 0 | 0 | 0 | 0 | 0 |
| Molar flow (kmol/h) | 20 | 20 | 41.3 | 100.3 | 100.2 | 20.0 | 0 |
| Mass flow (kg/h) | 1842 | 1842 | 3061 | 7413 | 5137 | 4118 | 15 |
| Component Flowrates in (kmol/h) | | | | | | | |
| Glycerol | 20.0 | 20.0 | 0.0 | 0.0 | 0.0 | 0.1 | 0.2 |
| TBA | 0.0 | 0.0 | 41.3 | 99.9 | 59.2 | 0.0 | 0.0 |
| MTBG | 0.0 | 0.0 | 0.0 | 0.0 | 0.1 | 0.0 | 0.0 |
| DTBG | 0.0 | 0.0 | 0.0 | 0.0 | 0.0 | 18.9 | 0.0 |
| TTBG | 0.0 | 0.0 | 0.0 | 0.0 | 0.0 | 1.0 | 0.0 |
| Water | 0.0 | 0.0 | 0.0 | 0.4 | 41.0 | 0.0 | 0.0 |
| Stream | 8 | 9 | 10 | 11 | 12 | 13 | |
| Temperature (K) | 308 | 371 | 360 | 464 | 364 | 308 | |
| Pressure (bar) | 1 | 2 | 1 | 2 | 1 | 1 | |
| Enthalpy flow (kW) | −27,695 | −8670 | −5619 | −29,369 | −3265 | −27,665 | |
| Vapor mole fraction | 0 | 0 | 0 | 0 | 0 | 0 | |
| Molar flow (kmol/h) | 149.7 | 100.3 | 59.0 | 191.4 | 41.4 | 149.8 | |
| Mass flow (kg/h) | 13,791 | 5137 | 4352 | 14,576 | 800 | 13,777 | |
| Component Flowrates in (kmol/h) | | | | | | | |
| Glycerol | 149.7 | 0.0 | 0.0 | 149.7 | 0.1 | 149.5 | |
| TBA | 0.0 | 59.2 | 58.6 | 0.6 | 0.6 | 0.0 | |
| MTBG | 0.0 | 0.1 | 0.0 | 0.1 | 0.1 | 0.0 | |
| DTBG | 0.0 | 0.0 | 0.0 | 0.0 | 0.0 | 0.0 | |
| TTBG | 0.0 | 0.0 | 0.0 | 0.0 | 0.0 | 0.0 | |
| Water | 0.3 | 41.0 | 0.4 | 41.0 | 40.6 | 0.3 | |

2.4. Process Integration

Heat integration has been conducted to reduce the energy requirements for the base case process. The integrated glycerol etherification process using reactive distillation is shown in Figure 13. Two heat exchangers have been added to the base-case process (E-103 and E-105) to generate medium-pressure steam (MPS-1 and MPS-2) to heat the T-101 reboiler.

The two heat exchangers use the bottom stream of RD and T-102 because of their high temperatures of 560 and 572 K, respectively. The product stream (stream 7) is also used to heat the feeds in E-101 and E-102 at 363 K. The product (stream 8) is cooled in heat exchanger E-104. The product stream exiting the reactive distillation is used to heat the feed streams of glycerol and TBA in E-101 and E-102 instead of using a steam utility. The stream information of the integrated process is shown in Table 6.

Table 6. Stream information of the integrated glycerol etherification process.

| Stream | 1 | 2 | 3 | 4 | 5 | 6 |
|--|-------|---------|-------|---------|---------|-------|
| Temperature (K) | 298 | 363 | 298 | 363 | 391 | 560 |
| Pressure (bar) | 1 | 5 | 1 | 5 | 4 | 4 |
| Enthalpy flow (kW) | −3708 | −3635 | −4119 | −9530 | −8670 | −3499 |
| Vapor mole fraction | 0 | 0 | 0 | 0 | 0 | 0 |
| Molar flow (kmol/h) | 20 | 20 | 41.3 | 100.3 | 100.3 | 20.0 |
| Mass flow (kg/h) | 1842 | 1842 | 3061 | 7413 | 5137 | 4118 |
| Component Flowrates in (kmol/h) | | | | | | |
| Glycerol | 20.0 | 20.0 | 0.0 | 0.0 | 0.0 | 0.1 |
| TBA | 0.0 | 0.0 | 41.3 | 99.9 | 59.2 | 0.0 |
| MTBG | 0.0 | 0.0 | 0.0 | 0.0 | 0.1 | 0.0 |
| DTBG | 0.0 | 0.0 | 0.0 | 0.0 | 0.0 | 18.9 |
| TTBG | 0.0 | 0.0 | 0.0 | 0.0 | 0.0 | 1.0 |
| Water | 0.0 | 0.0 | 0.0 | 0.4 | 41.0 | 0.0 |
| Stream | 7 | 8 | 9 | 10 | 11 | 12 |
| Temperature (K) | 476 | 374 | 308 | 298 | 308 | 371 |
| Pressure (bar) | 2 | 2 | 2 | 1 | 1 | 2 |
| Enthalpy flow (kW) | −3769 | −4048 | −4201 | −30 | −27,695 | −8670 |
| Vapor mole fraction | 0 | 0 | 0 | 0 | 0 | 0 |
| Molar flow (kmol/h) | 20.0 | 20.0 | 20.0 | 0.2 | 150.0 | 100.3 |
| Mass flow (kg/h) | 4118 | 4118 | 4118 | 15 | 13,791 | 5137 |
| Component Flowrates in (kmol/h) | | | | | | |
| Glycerol | 0.1 | 0.1 | 0.1 | 0.2 | 149.7 | 0.0 |
| TBA | 0.0 | 0.0 | 0.0 | 0.0 | 0.0 | 59.2 |
| MTBG | 0.0 | 0.0 | 0.0 | 0.0 | 0.0 | 0.1 |
| DTBG | 18.9 | 18.9 | 18.9 | 0.0 | 0.0 | 0.0 |
| TTBG | 1.0 | 1.0 | 1.0 | 0.0 | 0.0 | 0.0 |
| Water | 0.0 | 0.0 | 0.0 | 0.0 | 0.3 | 41.0 |
| Stream | 13 | 14 | 15 | 16 | 17 | |
| Temperature (K) | 360 | 464 | 364 | 572 | 308 | |
| Pressure (bar) | 1 | 2 | 1 | 1 | 1 | |
| Enthalpy flow (kW) | −5619 | −29,369 | −3265 | −25,051 | −27,665 | |
| Vapor mole fraction | 0 | 0 | 0 | 0 | 0 | |
| Molar flow (kmol/h) | 59.0 | 191.4 | 41.4 | 149.8 | 149.8 | |
| Mass flow (kg/h) | 4352 | 14576 | 800 | 13777 | 13777 | |
| Component Flowrates in (kmol/h) | | | | | | |
| Glycerol | 0.0 | 149.7 | 0.1 | 149.5 | 149.5 | |
| TBA | 58.6 | 0.6 | 0.6 | 0.0 | 0.0 | |
| MTBG | 0.0 | 0.1 | 0.1 | 0.0 | 0.0 | |
| DTBG | 0.0 | 0.0 | 0.0 | 0.0 | 0.0 | |
| TTBG | 0.0 | 0.0 | 0.0 | 0.0 | 0.0 | |
| Water | 0.4 | 41.0 | 40.6 | 0.3 | 0.3 | |

A comparison of the energy requirements between the base-case process and the improved process is shown in Figure 14a. The improved process can reduce total energy requirements by 17%. This is because the low-pressure steam was eliminated in the first two heat exchangers (E-101 and E-102), and the medium-pressure steam was generated within the process. A comparison of the CO₂ emissions of the base case and the improved process is shown in Figure 14b. The CO₂ emissions are reduced from 1898 kg/h in the base-case process to 1636.8 kg/h in the integrated process when natural gas is used to generate steam.

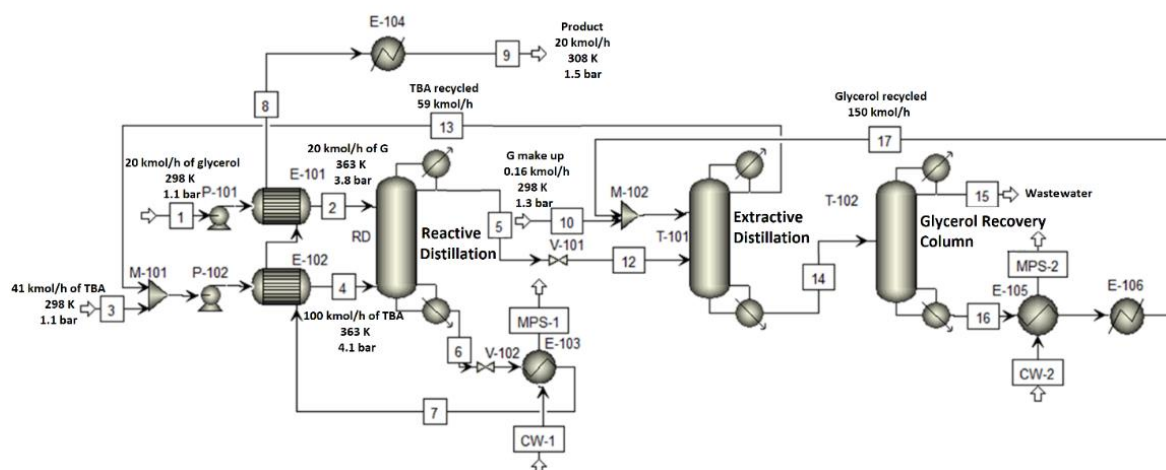


Figure 13. Heat-integrated process flow diagram (PFD) of glycerol etherification with TBA by reactive distillation.

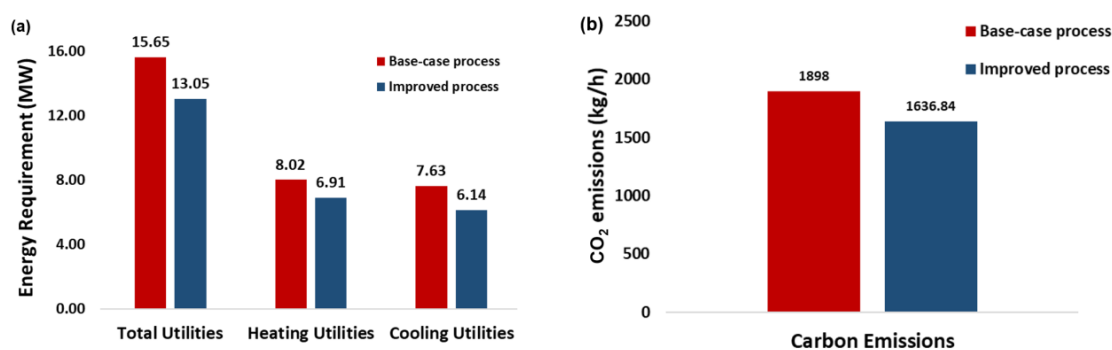


Figure 14. Comparison between the base-case and integrated processes of, (a) energy requirements, and (b) carbon emissions.

2.5. Economic Analysis

An economic evaluation was performed to check the profitability of the improved glycerol etherification process. Figure 15 shows the cost distribution of the main process equipment. The reactive distillation column is responsible for about 49% of the total cost. The extractive distillation column and solvent recovery column represent 25 and 17% of the total cost, respectively. Table 7 shows the prices of the raw materials, products, and utilities used in the process. The total annual cost of utilities is estimated at \$1,600,000. The cost distribution of the utilities is shown in Figure 16. The cost of high-pressure steam (hps) is accountable for ~65% of the total annual costs of utilities. The total production cost (TPC) was estimated to be \$43,860,000. The cost of raw materials is responsible for ~76.7% of the TPC.

Table 7. Materials and utility costs for glycerol etherification process [28,29].

| Item | Price |
|---|-------|
| Glycerol (\$/metric ton) | 445 |
| TBA (\$/metric ton) | 1150 |
| Product (\$/metric ton) | 1700 |
| Utilities | |
| Medium pressure steam (mps) (\$/metric ton) | 6 |
| High pressure steam (hps) (\$/metric ton) | 8 |
| Electricity (\$/kWh) | 0.045 |
| Cooling water (\$/m ³) | 0.08 |

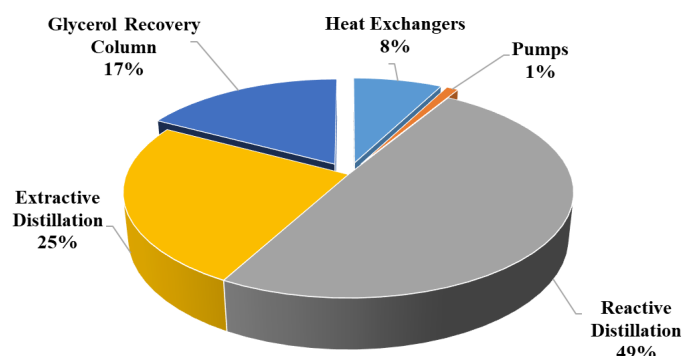


Figure 15. Purchased costs distribution of the main equipment for the glycerol etherification process based on reactive distillation.

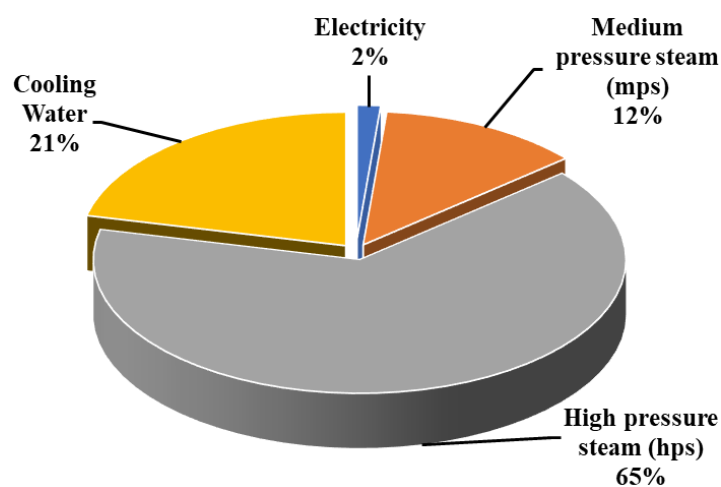


Figure 16. Costs distribution of utilities for glycerol etherification process.

Figure 17 shows the annual cost distribution of the total production cost of the glycerol etherification process. The direct costs, which are largely contributed by the raw materials costs, are responsible for 87% of the TPC, while the fixed charges and general expenses are responsible for the other 13%. The total capital cost of the investment is ~\$7,391,000, and the details of the calculations of the total investment cost are provided in Table 8 [30]. The economic evaluation summary of the reactive distillation-based process for glycerol etherification is shown in Table 9.

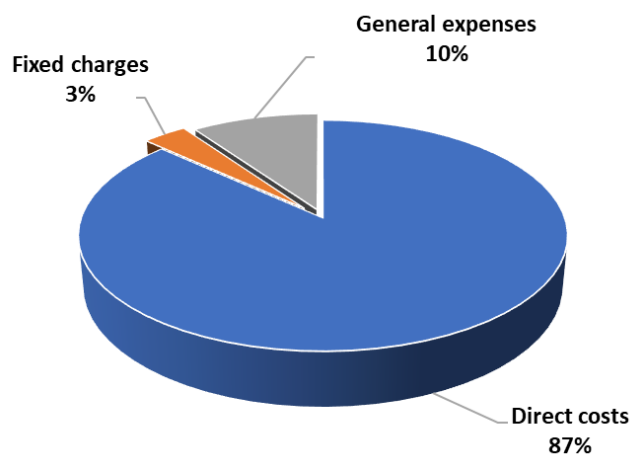


Figure 17. Annual cost distribution of TPC of the glycerol etherification process.

Table 8. Details of total capital investment calculations [29].

| | Fraction of Delivered Equipment for the Fluid Processing Plant | Calculated Values (million \$) |
|--|--|--------------------------------|
| Direct Costs | | |
| Purchased equipment, E' | | 1.133 |
| Delivery, a fraction of E' | 0.1 | 0.113 |
| Subtotal: delivered equipment | | 1.246 |
| Purchased equipment installation | 0.47 | 0.586 |
| Instrumentation & Controls (installed) | 0.36 | 0.449 |
| Piping (installed) | 0.68 | 0.847 |
| Electrical systems (installed) | 0.11 | 0.137 |
| Buildings (including services) | 0.18 | 0.224 |
| Yard improvements | 0.1 | 0.125 |
| Service facilities (installed) | 0.7 | 0.872 |
| Total direct costs | 2.6 | 4.487 |
| Indirect Costs | | |
| Engineering and supervision | 0.33 | 0.411 |
| Construction expenses | 0.41 | 0.511 |
| Legal expenses | 0.04 | 0.05 |
| Contractor's fee | 0.22 | 0.274 |
| Contingency | 0.44 | 0.548 |
| Total indirect costs | 1.44 | 1.795 |
| Fixed capital investment (FCI) | | 6.281 |
| Working capital (WC) | 0.89 | 1.109 |
| Total capital investment (TCI) | | 7.391 |

Table 9. Economic evaluation summary of the reactive distillation-based process for glycerol etherification.

| Item | Value |
|---|-------------|
| Fixed capital cost | \$6,282,000 |
| Total capital cost | \$7,391,000 |
| Return on investment (ROI) | 29.36% |
| Payback period | 2.2 |
| Net present value | \$7,853,000 |
| The discounted cash flow rate of return | 15.18% |

3. Materials and Methods

3.1. Chemicals

All reagents were obtained from a commercial source and used without prior treatment. Glycerol ($\geq 99.5\%$), *tert*-butanol ($\geq 99\%$), SnCl_2 (98%), and $\text{H}_3\text{PMo}_{12}\text{O}_{40}$ were purchased from Sigma Aldrich (St. Louis, MO, USA). Dodecane (99%,) was purchased from Vetec (Sigma Aldrich, St. Louis, MO, USA). The Sn (II)-phosphomolybdate catalysts ($\text{Sn}_{1.5}\text{PMo}_{12}\text{O}_{40}$) were synthesized in the lab [24].

3.2. Synthesis of Catalysts

All the catalyst salts were synthesized according to the literature [15]. Typically, an aqueous solution (ca. 5 mL) of stannous chloride at an adequate stoichiometry was slowly dropped into another solution (ca. 20 mL) containing the solved $\text{H}_3\text{PMo}_{12}\text{O}_{40}$. The resulting suspension was magnetically stirred and heated at 333 K/3h. Afterward, the solvent was evaporated at 383 K, and the salt obtained was dried in an oven at 423 K/5 h and posteriorly calcined at 573 K/5 h.

3.3. Characterizations of $\text{Sn}_{1.5}\text{PMo}_{12}\text{O}_{40}$ Catalyst

SEM images and EDS analysis were performed in a JEOL JSM 6010LA microscope (Tokyo, Japan) from secondary electrons imaging (SEI) at 10 mm of work distance, electron source at 20 kV, and $1500\times$ magnification.

Diffraction patterns were recorded in a Bruker D8 Discover diffractometer (Billerica, MA, USA), operating with Cu-K α radiation and a Ni filter, at 40 kV and 40 mA.

Porosity analyses were done through the DFT method in a NOVA 1200 Quantachrome instrument (Boynton Beach, FL, USA). N_2 adsorption/desorption isotherms were acquired at 77 K, after samples were degassed in a vacuum at 383 K/5 h. The surface area was determined from the BET method applied to the isotherms with P/P $_0$ varying from 0.05 to 0.32.

FTIR spectra were collected by the Attenuate Total Reflectance method in a Varian 660-IR instrument (Middelburg, The Netherlands), coupled to a PIKE Technologies GladiATR-TRTM accessory (Madison, WI, USA).

3.4. Catalytic Runs

The catalytic experimental runs of glycerol etherification with TBA were conducted in a sealed tube reactor (35 mL) equipped with a magnetic stirrer, and the reactor was placed in a thermostatic oil bath. Glycerol (0.84 mM), *tert*-butyl alcohol (3.37 mM), and dodecane as an internal standard (0.1 mM) were added to the reactor. The system was stirred for 5 min and heated to 363 K. Afterward, an exact amount of catalyst (9.2×10^{-4} mM, 0.2 mol% Sn (II) ions) was added to the reaction and monitored for 240 min.

3.5. Conversion and Selectivity

Glycerol and *tert*-butyl ethers were analyzed in a Shimadzu CG-2010 plus, equipped with a capillary Carbowax 20 M (30 m \times 0.25 mm \times 0.25 μm) column and FID detector. The column temperature started at 80 $^\circ\text{C}$ and was raised to 210 $^\circ\text{C}$ (10 $^\circ\text{C}/\text{min}$). The injector and detector were set to 250 $^\circ\text{C}$. The carrier gas was H_2 . A split ratio of 1:30 was used.

To determine the response factor of the products, glycerol ethers were previously separated from the reaction medium through chromatography in a silica column, using ethyl acetate, chloroform, and methanol as eluents at different proportions. The response factors concerning glycerol were 7.3, 5.3, and 3.1 for TTBG, DTBG, and MTBG, respectively.

The conversion of glycerol was estimated through gas chromatography analysis of aliquots collected periodically to compare the amount of glycerol consumed to the initial glycerol concentration at different time intervals. The main products were identified by GC-MS analysis (GC-MS 2010 ultra-mass, operating at 70 eV). The reaction products were identified through co-injection in GC equipment with authentic samples that were previously synthesized in the lab [24]. The compositions of reactants and products at different reaction temperatures are illustrated in Table 10. The experimental conditions were: glycerol (4.6 mmol), TBA (36.8 mmol), catalyst (0.2 mol% of Sn^{2+} , 195 mg of $\text{Sn}_{1.5}\text{PMo}_{12}\text{O}_{40}$), temperatures (353, 363, 373 and 383 K), time (4 h), internal standard (dodecane 0.100 mL), total volume (4 mL).

Table 10. Initial and final compositions at different temperatures.

| Temperature K | Moles of Glycerol | | Moles of Products | | | Moles of TBA | |
|---------------|-------------------|--------|-------------------|--------|--------|--------------|--------|
| | 0h | 4h | MTBG | DTBG | TTBG | 0 h | 4 h |
| 353 | 0.0046 | 0.0013 | 0.0026 | 0.0005 | 0.0000 | 0.0368 | 0.0333 |
| 363 | 0.0046 | 0.0011 | 0.0027 | 0.0008 | 0.0000 | 0.0368 | 0.0325 |
| 373 | 0.0046 | 0.0012 | 0.0024 | 0.0010 | 0.0001 | 0.0368 | 0.0323 |
| 383 | 0.0046 | 0.0014 | 0.0023 | 0.0007 | 0.0000 | 0.0368 | 0.0331 |

3.6. Reaction Pathway

The reaction pathway of glycerol etherification with TBA is depicted according to the literature [4]. A kinetic model of the glycerol etherification with TBA over the $\text{Sn}_{1.5}\text{PMo}_{12}\text{O}_{40}$ catalyst was derived by the lumping approach [7,8]. The kinetic model corresponds to the scheme shown in Figure 18.

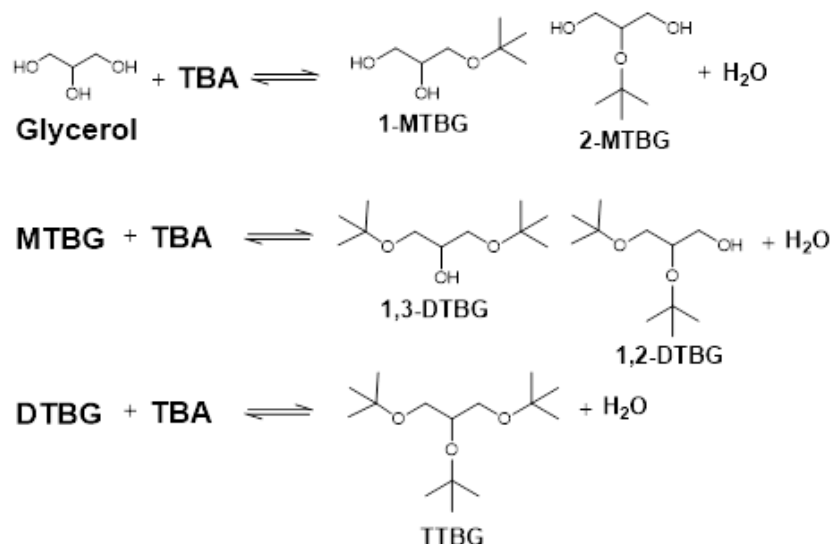


Figure 18. Glycerol etherification reactions with TBA.

It is important to note that TBA can undergo dehydration, leading to the formation of isobutylene, which could react with glycerol through another reaction pathway. It was verified that by using TBA in excess and a temperature of 363 K, the TBA concentration in the gas phase remains almost unaltered. This reaction can be minimized by having little or no impact on the overall process [25].

The reactions yield mono-*tert*-butyl glycerol (MTBG), di-*tert*-butyl glycerol (DTBG), and tri-*tert*-butyl glycerol (TTBG). In the first step, glycerol reacts with TBA to produce MTBG and water. MTBG produced from the first step reacts with TBA to produce DTBG and water. DTBG reacts with TBA in the third step to produce TTBG and water.

The equilibrium behavior of the etherification reactions was studied using the REquil reactor model embedded in Aspen Plus. The REquil model calculates the reaction equilibrium constants (K_{eq}) from the Gibbs free energy of the participating components [31]. The equilibrium constants are functions of the temperature.

The compositions at the thermodynamic equilibrium for etherification reactions were evaluated at different temperatures and compared with the data obtained experimentally, as shown in Figure 19. It was noticed that the conversion of glycerol at the thermodynamic equilibrium reached more than 99.99% at all temperatures, with a very slight decrease in conversion when increasing the temperature. However, the maximum glycerol conversion achieved experimentally was 76% at 363 K after 4 h of reaction time. As shown in Figure 19a, there are large differences between the equilibrium values and the experimental data, indicating that the etherification reaction is limited by kinetics.

Figure 19b shows that only MTBG and DTBG are present in the product distribution obtained experimentally, and only a small amount of TTBG is present. In contrast, the selectivity of TTBG is almost 100% across all temperatures at the thermodynamic equilibrium.

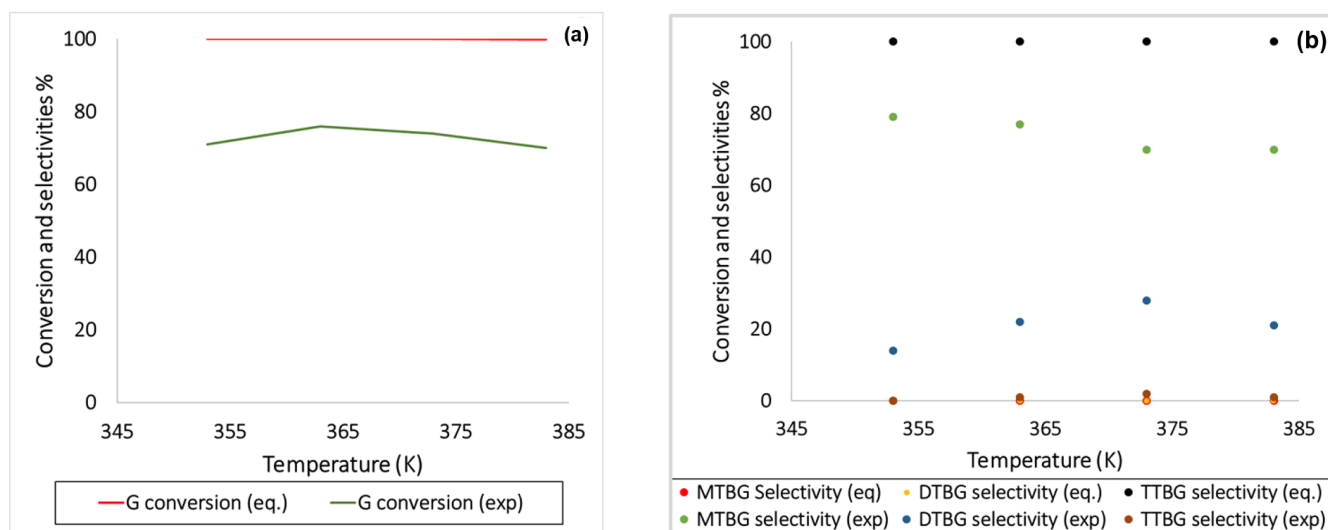


Figure 19. Experimental and equilibrium values of, (a) Glycerol conversion as a function of temperature, (b) Component selectivity as a function of temperature.

4. Conclusions

In this work, a kinetic model for glycerol etherification with TBA over $\text{Sn}_{1.5}\text{PMo}_{12}\text{O}_{40}$ catalyst has been developed using the lumping approach. The kinetic model is proved to be valid since the simulation results are in good agreement with the actual experimental data. A reactive distillation column was designed and optimized to produce glycerol ethers with the highest purity of 99.5% and a glycerol conversion of ~99%. The achieved results were obtained using a lower TBA to glycerol feed ratio as compared to the conventional process. A reactive distillation-based process was developed for glycerol etherification to produce 33,000 metric tons per year of glycerol ethers. The energy requirements for the process were reduced by implementing heat integration into the process, and the energy requirements and CO_2 emissions were reduced by 17% and 14%, respectively. An economic analysis was carried out to evaluate the profitability of the glycerol etherification process, and it was found that the process is profitable, with a return on investment of 29.4% and a payback period of 2.2 years.

Author Contributions: Conceptualization: A.A.A.-R. and M.J.d.S.; methodology: A.A.A.-R.; formal analysis and investigation: A.A.A.-R., R.K.A.D., A.E.A., D.M.C. and M.J.d.S.; visualization: R.K.A.D., A.E.A. and D.M.C.; writing—original draft preparation: A.A.A.-R., R.K.A.D. and M.J.d.S.; writing—review and editing: A.A.A.-R. and M.J.d.S.; funding acquisition: A.A.A.-R. and M.J.d.S.; resources: A.A.A.-R. and M.J.d.S.; supervision: A.A.A.-R. and M.J.d.S. All authors have read and agreed to the published version of the manuscript.

Funding: This research received no external funding.

Data Availability Statement: Not applicable.

Acknowledgments: This study was supported by King Saud University, Deanship of Scientific Research, College of Engineering Research Center. The authors are grateful for the support from CNPq and FAPEMIG (Brasil). This study was also partially funded by the Coordenação de Aperfeiçoamento de Pessoal de Nível Superior—Brasil (CAPES)—Finance Code 001.

Conflicts of Interest: The authors declare no conflict of interest.

Nomenclature

| | |
|------------------|---|
| C_i | Concentration of component i, mol/m ³ |
| E_a | Activation Energy, kJ/mol |
| k_{0_i} | Pre exponential factor of reaction i, m ³ /mol.s |
| k_i | Reaction i rate constant, m ³ /mol.s |
| r_i | Reaction i rate, mol/(m ³ s) |
| R | Gas constant, kJ/(mol K) |
| T | Temperature, K |
| Subscripts | |
| DTBG | Di- <i>tert</i> -butyl glycerol |
| G | Glycerol |
| H ₂ O | Water |
| MTBG | Mono- <i>tert</i> -butyl glycerol |
| RD | Reactive distillation |
| TBA | <i>Tert</i> -butyl alcohol |
| TTBG | Tri- <i>tert</i> -butyl glycerol |

References

- Campo, L.; Rossella, F.; Mercadante, R.; Fustinoni, S. Exposure to BTEX and Ethers in Petrol Station Attendants and Proposal of Biological Exposure Equivalents for Urinary Benzene and MTBE. *Ann. Occup. Hyg.* **2016**, *60*, 318–333. [\[CrossRef\]](#) [\[PubMed\]](#)
- Li, D.; Liu, Q.; Gong, Y.; Huang, Y.; Han, X. Cytotoxicity and Oxidative Stress Study in Cultured Rat Sertoli Cells with Methyl *Tert*-Butyl Ether (MTBE) Exposure. *Reprod. Toxicol.* **2009**, *27*, 170–176. [\[CrossRef\]](#)
- Moran, M.J.; Zogorski, J.S.; Squillace, P.J. MTBE and Gasoline Hydrocarbons in Ground Water of the United States. *Ground Water* **2005**, *43*, 615–627. [\[CrossRef\]](#)
- Karinen, R.S.; Krause, A.O.I. New Biocomponents from Glycerol. *Appl. Catal. A Gen.* **2006**, *306*, 128–133. [\[CrossRef\]](#)
- Subhash, M.; Pal, D.B.; Jana, S.K. Biofuels Additives Derived via Clay Supported Heteropoly Acid Catalyzed Etherification of Glycerol with T-Butanol-Biomass to Liquid Oxygenates. *Chem. Pap.* **2022**, *76*, 775–784. [\[CrossRef\]](#)
- Marulanda, V.F. Biodiesel Production by Supercritical Methanol Transesterification: Process Simulation and Potential Environmental Impact Assessment. *J. Clean Prod.* **2012**, *33*, 109–116. [\[CrossRef\]](#)
- Bozbas, K. Biodiesel as an Alternative Motor Fuel: Production and Policies in the European Union. *Renew. Sustain. Energy Rev.* **2008**, *12*, 542–552. [\[CrossRef\]](#)
- Frusteri, F.; Arena, F.; Bonura, G.; Cannilla, C.; Spadaro, L.; di Blasi, O. Catalytic Etherification of Glycerol by *Tert*-Butyl Alcohol to Produce Oxygenated Additives for Diesel Fuel. *Appl. Catal. A Gen.* **2009**, *367*, 77–83. [\[CrossRef\]](#)
- Meher, L.C.; Vidya Sagar, D.; Naik, S.N. Technical Aspects of Biodiesel Production by Transesterification—A Review. *Renew. Sustain. Energy Rev.* **2006**, *10*, 248–268. [\[CrossRef\]](#)
- Pico, M.P.; Romero, A.; Rodr, S.; Santos, A. Etherification of Glycerol by *Tert*-Butyl Alcohol: Kinetic Model. *Ind. Eng. Chem. Res.* **2012**, *51*, 9500–9509. [\[CrossRef\]](#)
- Melero, J.A.; Vicente, G.; Paniagua, M.; Morales, G.; Muñoz, P. Etherification of Biodiesel-Derived Glycerol with Ethanol for Fuel Formulation over Sulfonic Modified Catalysts. *Bioresour. Technol.* **2012**, *103*, 142–151. [\[CrossRef\]](#) [\[PubMed\]](#)
- Jaworski, M.A.; Rodríguez Vega, S.; Siri, G.J.; Casella, M.L.; Romero Salvador, A.; Santos López, A. Glycerol Etherification with Benzyl Alcohol over Sulfated Zirconia Catalysts. *Appl. Catal. A Gen.* **2015**, *505*, 36–43. [\[CrossRef\]](#)
- Pico, M.P.; Rodríguez, S.; Santos, A.; Romero, A. Etherification of Glycerol with Benzyl Alcohol. *Ind. Eng. Chem. Res.* **2013**, *52*, 14545–14555. [\[CrossRef\]](#)
- Liu, J.; Zhang, Z.; Zhang, P.; Yang, B. On the Kinetics of Multiphase Etherification of Glycerol with Isobutene. *Chem. Eng. J.* **2019**, *375*, 122037. [\[CrossRef\]](#)
- Chaves, D.M.; Ferreira, S.O.; Chagas da Silva, R.; Natalino, R.; da Silva, M. Glycerol Esterification over Sn (II)-Exchanged Keggin Heteropoly Salt Catalysts: Effect of Thermal Treatment Temperature. *Energy Fuels* **2019**, *33*, 7705–7716. [\[CrossRef\]](#)
- Klepáčová, K.; Mravec, D.; Kaszonyi, A.; Bajus, M. Etherification of Glycerol and Ethylene Glycol by Isobutylene. *Appl. Catal. A Gen.* **2007**, *328*, 1–13. [\[CrossRef\]](#)
- Pico, M.P.; Rosas, J.M.; Rodríguez, S.; Santos, A.; Romero, A. Glycerol Etherification over Acid Ion Exchange Resins: Effect of Catalyst Concentration and Reusability. *J. Chem. Technol. Biotechnol.* **2013**, *88*, 2027–2038. [\[CrossRef\]](#)
- Chang, J.S.; Chen, D.H. Optimization on the Etherification of Glycerol with *Tert*-Butyl Alcohol. *J. Taiwan Inst. Chem. Eng.* **2011**, *42*, 760–767. [\[CrossRef\]](#)
- Lee, H.J.; Seung, D.; Filimonov, I.N.; Kim, H. Etherification of Glycerol by Isobutylene. Effects of the Density of Acidic Sites in Ion-Exchange Resin on the Distribution of Products. *Korean J. Chem. Eng.* **2011**, *28*, 756–762. [\[CrossRef\]](#)
- Lee, H.J.; Seung, D.; Jung, K.S.; Kim, H.; Filimonov, I.N. Etherification of Glycerol by Isobutylene: Tuning the Product Composition. *Appl. Catal. A Gen.* **2010**, *390*, 235–244. [\[CrossRef\]](#)

21. González, M.D.; Cesteros, Y.; Salagre, P. Establishing the Role of Brønsted Acidity and Porosity for the Catalytic Etherification of Glycerol with *Tert*-Butanol by Modifying Zeolites. *Appl. Catal. A Gen.* **2013**, *450*, 178–188. [CrossRef]
22. Celdeira, P.A.; Gonçalves, M.; Figueiredo, F.C.A.; Bosco, S.M.D.; Mandelli, D.; Carvalho, W.A. Sulfonated Niobia and Pillared Clay as Catalysts in Etherification Reaction of Glycerol. *Appl. Catal. A Gen.* **2014**, *478*, 98–106. [CrossRef]
23. Manjunathan, P.; Kumar, M.; Churipard, S.R.; Sivasankaran, S.; Shanbhag, G.v.; Maradur, S.P. Catalytic Etherification of Glycerol to *Tert*-Butyl Glycerol Ethers Using *Tert*-Butanol over Sulfonic Acid Functionalized Mesoporous Polymer. *RSC Adv.* **2016**, *6*, 82654–82660. [CrossRef]
24. da Silva, M.J.; Chaves, D.M.; ferreira, S.O.; da Silva, R.C.; Gabriel Filho, J.B.; Bruziquesi, C.G.O.; Al-Rabiah, A.A. Impacts of Sn(II) Doping on the Keggin Heteropolyacid-Catalyzed Etherification of Glycerol with *Tert*-Butyl Alcohol. *Chem. Eng. Sci.* **2022**, *247*, 116913. [CrossRef]
25. Kiss, A.A.; Jobson, M.; Gao, X. Reactive Distillation: Stepping Up to the Next Level of Process Intensification. *Ind. Eng. Chem. Res.* **2019**, *58*, 5909–5918. [CrossRef]
26. Kiss, A.A. Distillation Technology—Still Young and Full of Breakthrough Opportunities. *J. Chem. Technol. Biotechnol.* **2014**, *89*, 479–498. [CrossRef]
27. Kiatkittipong, W.; Intarachoen, P.; Laosiripojana, N.; Chaisuk, C.; Praserttham, P.; Assabumrungrat, S. Glycerol Ethers Synthesis from Glycerol Etherification with *Tert*-Butyl Alcohol in Reactive Distillation. *Comput. Chem. Eng.* **2011**, *35*, 2034–2043. [CrossRef]
28. International Trade Center. Available online: <https://www.Trademap.Org/Index.Asp> (accessed on 20 March 2022).
29. Comex Stat. Available online: <Http://Comexstat.Mdic.Gov.Br/> (accessed on 20 March 2022).
30. Peters, M.S.; Timmerhaus, K.D.; West, R.E. *Plant Design and Economics for Chemical Engineers*; McGraw-Hill: New York, NY, USA, 2003; Volume 4.
31. Al-Malah, K.I.M. *Aspen Plus: Chemical Engineering Applications*; John Wiley & Sons: Hoboken, NJ, USA, 2016.